



The Morávka meteorite fall: 2. Interpretation of infrasonic and seismic data

P. G. BROWN,^{1*} P. KALENDA,² D. O. REVELLE,³ and J. BOROVIČKA⁴

¹Department of Physics and Astronomy, University of Western Ontario, London, Ontario N6A 3K7, Canada

²CoalExp, Kosmonautu 2, 70030 Ostrava 3, The Czech Republic

³Los Alamos National Laboratory, P.O. Box 1663, MS J557, Los Alamos, New Mexico 87545, USA

⁴Astronomical Institute of the Academy of Sciences, 25165 Ondřejov, The Czech Republic

*Corresponding author. E-mail: pbrown@uwo.ca

(Received 06 September 2002; revision accepted 19 June 2003)

Abstract—The sound production from the Morávka fireball has been examined in detail making use of infrasound and seismic data. A detailed analysis of the production and propagation of sonic waves during the atmospheric entry of the Morávka meteoroid demonstrates that the acoustic energy was produced both by the hypersonic flight of the meteoroid (producing a cylindrical blast wave) and by individual fragmentation events of the meteoroid, which acted as small explosions (producing quasi-spherical shock waves). The deviation of the ray normals for the fragmentation events was found to be as much as 30° beyond that expected from a purely cylindrical line source blast. The main fragmentation of the bolide was confined to heights above 30 km with a possible maximum in acoustic energy production near 38 km. Seismic stations recorded both the direct arrival of the airwaves (the strongest signal) as well as air-coupled P-waves and Rayleigh waves (earlier signals). In addition, deep underground stations detected the seismic signature of the fireball. The seismic data alone permit reconstruction of the fireball trajectory to a precision on the order of a few degrees. The velocity of the meteoroid is much less well-determined by these seismic data. The more distant infrasonic station detected 3 distinct signals from the fireball, identified as a thermospheric return, a stratospheric return, and an unusual mode propagating through the stratosphere horizontally and then leaking to the receiver.

INTRODUCTION

The Morávka meteorite fall is undoubtedly the most documented in history. This ordinary chondrite fell on May 6, 2000 in the Czech Republic while the passage of the fireball through the atmosphere was recorded by videographers, visual observers, infrasonic microphones, seismographs on the ground, and by satellites in orbit. Reconstruction of the fireball trajectory and initial velocity upon entry (Borovička et al. 2003a) has permitted accurate determination of the pre-fall orbit, only the seventh meteorite orbit to date. Analysis of these fireball data together with laboratory analysis of the recovered meteorites (see Borovička et al. 2003b) has facilitated analysis of the orbital evolution of the Morávka meteoroid, while measurement of the initial mass of the pre-atmospheric body by 4 independent methods has enabled cross-calibrations of these various techniques. Analysis of video recordings in combination with seismic data has also provided, for the first time, observational measurements of

high spatial and temporal resolution relating to the fragmentation behavior of a large body entering the Earth's atmosphere (Borovička and Kalenda 2003).

As part of the broad interdisciplinary study of the Morávka meteorite fall, this work focuses on the sound production accompanying the fireball. By understanding the acoustic processes present in Morávka, we hope to establish the observational baseline for the interpretation of other fireball acoustic data where much less information may be available. The acoustic energy budget is part of the broader energy balance associated with the entry of large meteoroids (cf., Ceplecha et al. 1998), and insight into its behavior is a key component to understanding the overall entry behavior of bodies into planetary atmospheres.

In particular, we examine infrasonic recordings (acoustic frequencies from 0.01–20 Hz) of the Morávka fireball and seismic data. These include infrasonic data from Freyung, Germany and seismic data from a large number of stations that recorded both direct acoustic arrivals and sound energy

converted to seismic waves. The amount of data in combination with such a well-known fireball trajectory has enabled analyses not done previously for any fireball. Of particular interest is establishment of the exact nature of the acoustic source production at the fireball. The prevailing theoretical models (cf., ReVelle 1976) suggest that if the sound is generated primarily by the ballistic shock accompanying the fireball's ablation, the behavior of the source should be that of a cylindrical line source. In contrast, if fragmentation is significant, one might expect the sound produced to be more similar to that of a moving point source. The primary difference between these 2 cases is that acoustic rays at the source propagate normal to the fireball trajectory for a cylindrical line source. In the case of a moving point source, rays may deviate significantly from this perpendicular condition, though the magnitude of this deviation has not yet been measured and likely depends on the nature and geometry of the associated fragmentation. However, the nature of such fragmentation events and constraints on the sources (height, deviation of rays from normal propagation, etc.) has not before been observationally determined with the precision possible for the Morávka fall. Additionally, a detailed understanding of the nature of the sound propagation, the atmospheric ducts involved, and the interpretation of the associated seismic records provide a unique opportunity to study effects caused by atmospheric propagation and to clearly separate these from source effects.

SEISMIC DATA: DESCRIPTION AND INTERPRETATION

In addition to the acoustic energy generated by the Morávka fireball and detected directly in the atmosphere by microbarographs, significant signal energy was transferred into seismic vibrations and registered by a large number of seismographs proximal to the fireball trajectory. Seismic

detections of bright fireballs are not exceptional (see e.g., Cumming 1989; Cevolani 1994; Brown et al. 2002b). In particular, Qamar (1995) showed, using the re-entry of the Space Shuttle as an example, that sonic waves can be used for the determination of the height and velocity for moderately supersonic objects.

From examination of the records of several seismic stations, Brown et al. (2002b) concluded that the Tagish Lake fireball produced some cylindrical shock waves in addition to possible quasi-spherical shocks produced from fragmentation events, while Anglin and Haddon (1987) were able to interpret the seismic signature of the airwave from a bright fireball near Yellowknife, Canada as due entirely to a cylindrical line-source shock. In contrast, the fireball associated with the Vilna meteorite fall detected by Folinsbee et al. (1969) produced most of its acoustic energy at the detonation near the end point of its trajectory as seen from one particular seismic station. Anglin and Haddon (1987) also demonstrated the generation of individual types of waves genetically related to the primary sonic blast wave from the Yellowknife fireball. Brown et al. (2002b) have shown that, in some cases, the first waves to arrive at a distant station are the P-waves generated by acoustic coupling near the subterminal point of the trajectory, where sound first reaches the earth's surface.

The above analyses were limited by either a low number or suboptimal distribution of seismic stations and/or incomplete knowledge of the fireball trajectory. The Morávka fireball, on the other hand, was registered at 16 seismic stations ranging from the immediate vicinity of the trajectory ground projection up to a distance of 180 km. The stations are listed in Table 1, and their positions are plotted in Fig. 1 together with the path of the fireball.

The fireball flew over the core of the Seismic Polygon OKD (Ostrava-Karvina mining district) operated by the DPB Paskov firm (J. Holečko, personal communication). The polygon is formed by 7 surface or near-surface stations and 3

Table 1. List of the seismic stations that detected the Morávka fireball.

Code	Location	Operator	Longitude (° E)	Latitude (° N)	Altitude (m)	Depth (m)
CSM	ČSM mine	DPB	18.5608	49.8004	278	0
RAJ	Karviná-Ráj	DPB	18.5817	49.8514	272	30
LUT	Orlová-Lutyne	DPB	18.4150	49.8832	217	30
PRS	Prstná	DPB	18.5528	49.9143	205	30
BMZ	Ostrava-Krásné Pole	DPB	18.1411	49.8344	250	17
HAV	Havířov	DPB	18.4763	49.7619	301	30
CHO	Chotebuz	DPB	18.5594	49.7682	301	30
MAJ	Máj mine	DPB	18.4713	49.8237	-365	575
CSA	ČSA mine	DPB	18.4925	49.8531	-497	717
KVE	Květen mine	DPB	18.5007	49.8003	-141	350
RAC	Racibórz	PAN	18.1905	50.0829	214	2
OJC	Ojców	PAN	19.7972	50.2187	300	0
VRAC	Vranov	MU	16.5888	49.3092	470	5
MORC	Moravský Beroun	MU	17.5458	49.7752	742	5
KRUC	Moravský Krumlov	MU	16.3939	49.0611	341	0
JAVC	Velká Javorina	MU	17.6695	48.8749	827	0

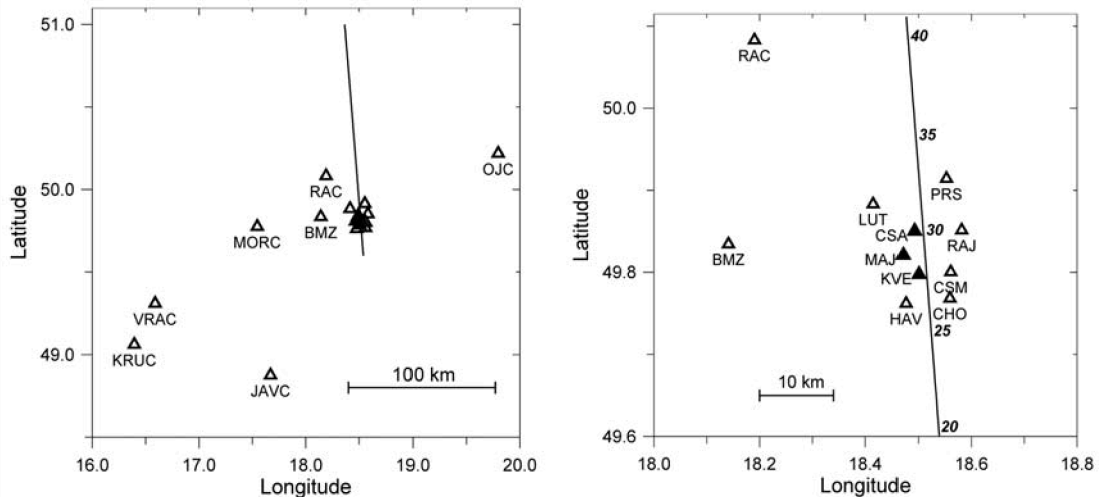


Fig. 1. Positions of seismic stations relative to the fireball trajectory as derived from the video records. The right panel represents a detailed view of the central part. Fireball altitudes in km are given in this part. Deep underground stations are plotted as filled triangles.

deep underground stations. Each station is equipped with a 3-component seismometer with a sampling frequency of 125 Hz. The digital recording is triggered after a seismic event is detected at a minimum of 5 stations. An 8-sec record is then written. For Morávka, the record starts at 11:53:18.744 UT (the station clocks are radio controlled). This time was too late for stations HAV and CHO, where the onset of the main signal is missing. A rough analogue record shows that the onset occurred here a few tenths of a second earlier. The digital record lasts for 1 min.

The fireball signal was also detected at 2 stations in Poland operated by the Polish Academy of Science (PAN; P. Wójcicki and W. Wojtak, personal communication). One of these stations (RAC) was only 20 km from the trajectory ground projection. Four stations operated by Masaryk University in Brno (MU; J. Pazdírková, personal communication) also detected the fireball. The sampling frequency at these stations was between 20 and 80 Hz.

By analyzing the seismic records, we were able to identify several types of waves most visible at those stations lying some distance from the fireball trajectory where arrival times are widely separated. At all stations, the first arrivals are air-coupled P-waves originating in the vicinity of trajectory terminal point (i.e., the point where most of the meteoroid mass became subsonic). This is the lowest point of the supersonic trajectory, and the waves from this point reach the ground first. At the point where their surface trace velocity is comparable to the surface P-wave velocity, they are transmitted into the ground (or, alternatively, they are refracted under the critical angle according to Snell's law (about 5°) and continue to the station as near-surface ground P-waves). Subsequently, P-waves from other, more distant points along the trajectory arrive.

The seismic records from stations BMZ and MORC are shown in Figs. 2 and 3, respectively. Both contain P-waves.

The strongest signal, however, is associated with the direct arrival of airwaves later on. These first airwaves come from the point along the trajectory nearest the station. They propagate as a cylindrical blast wave from the trajectory with a very small Mach cone angle, given by the ratio of fireball velocity to the speed of sound (see the section on cylindrical line source blast below). Near the end of the trajectory, where the velocity of the meteoroid becomes very low, the airwaves also propagate as a quasi-spherical wave to the stations lying downrange of the trajectory terminal point (VRAC, KRUC, JAVC). Of course, the actual shape of the wave is deformed by the varying speed of sound at various altitudes. The onset of the direct airwaves is always quite sharp in the seismic records, and the waves have high frequencies corresponding to acoustic frequencies (50–2000 Hz). Although the direct airwaves are under sampled on all stations, they are easily visible in the filtered signal (Fig. 3).

These direct airwaves are preceded by genetically related air-coupled Rayleigh waves, which are formed by the transformation of direct airwaves on the ground and moving along the surface. The amplitude of the Rayleigh waves gradually increases until the arrival of the airwaves (Fig. 2). Both types of waves can be distinguished clearly by the much lower frequencies of the Rayleigh waves.

In addition to the strong arrival of the blast wave, the direct airwave signal also contains numerous individual disturbances (sub-maxima). We interpret these as having been generated by various point sources along the trajectory. These sources are presumably connected with individual meteoroid fragmentation events. The acoustic waves propagate as spherical waves from the source, and the arrival time then depends on the distance to the station. We were able to localize a number of fragmentation events using their seismic signatures as described in more detail in Borovička and Kalenda (2003).

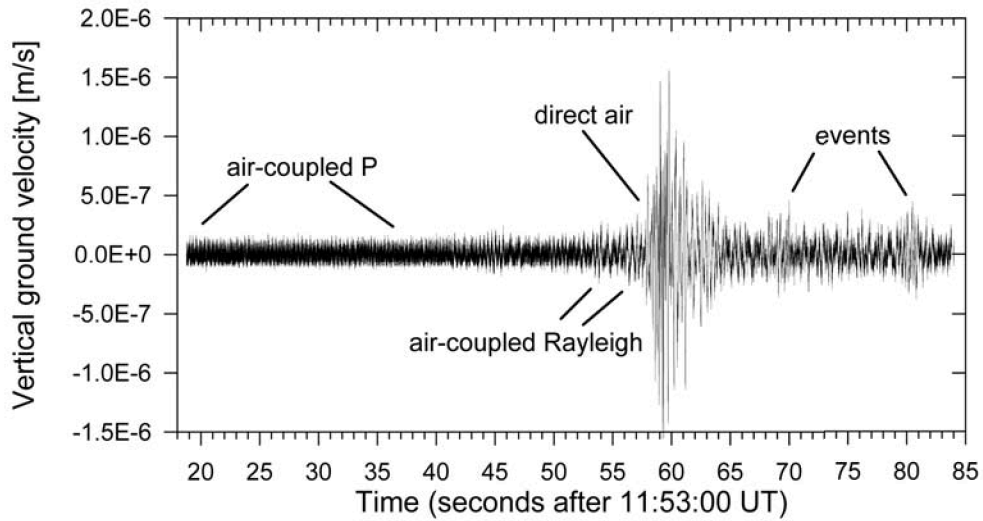


Fig. 2. Seismic record from station BMZ and the description of individual wave groups. The time is given in seconds after 11:53:00 UT. The first P-waves arrived before the start of the record.

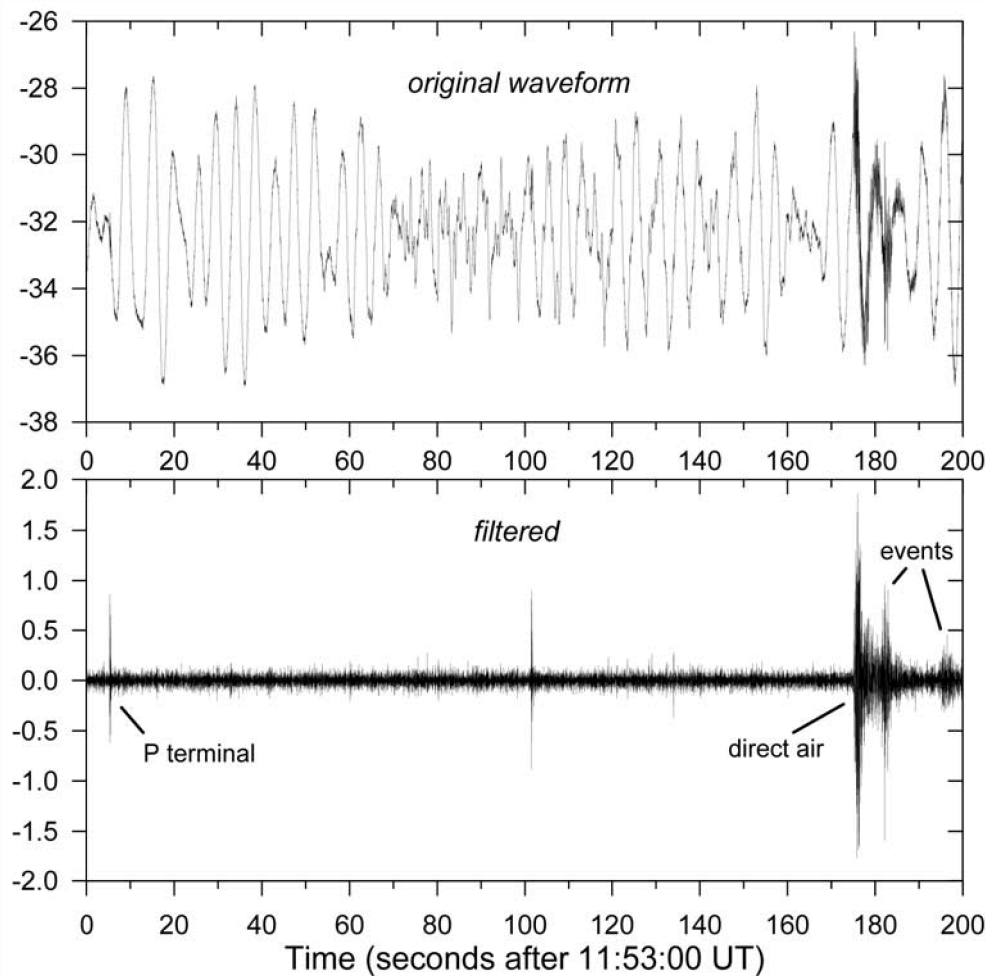


Fig. 3. Seismic record from station MORC and the description of individual wave groups. The original waveform is given in the upper plot. The filtered signal, with low frequencies (<25 Hz) removed, is in the lower plot.

Particular emphasis has been devoted to analysis of the seismic signals recorded in the deep underground stations. Here, P-waves are registered, having been generated by the refraction of the airwaves on the surface. A given ray coming to the underground station traverses smaller distances in the air than would be the case for detection at a station at the surface having the same coordinates. However, the ray still has to travel through the rock down to the station. Given that the P-wave signal velocity is typically 2–4 km/s in near-surface rock, we found that, in our case (with relatively shallow stations), these corrections are negligible, and the timing at the underground stations was, therefore, used without change with the station depths being ignored.

Table 2 provides the arrival times of different types of waves at each station. The signal at the distant stations was weak. Acoustic ray tracing showed that stations KRUC and JAVC lie almost in the acoustic shadow with most of the airwaves reflected above the surface. The identification of the P-type wave at station RAC is uncertain—the given time may, in fact, correspond to a seismic event not connected with the fireball.

To check our identifications of the direct airwaves and to demonstrate the internal consistency of the seismic data and our interpretations of it, we use the timings of the arrivals of direct airwaves to compute the fireball trajectory independent of the video data (cf., Borovička et al. 2003a). A similar approach was recently used independently by Ishihara et al. (2001), who also studied the correlation of shock wave amplitude with meteoroid mass. We used stations CSM, RAJ, LUT, PRS, BMZ, RAC, OJC, and MORC for trajectory computation. Stations VRAC, KRUC, and JAVC could not be used because they lie in the region where the cylindrical wave does not propagate. For a chosen initial latitude of 49.90° , we computed the following 7 free parameters of the trajectory: the remaining 2 coordinates of the initial point (longitude and altitude), the azimuth and slope of the trajectory, the time of fireball passage through the initial point (t_0), the velocity and deceleration of the fireball at that point. The procedure was iterative. Because the speed of sound changes with

temperature, i.e., altitude, we computed the average speed of sound from a particular altitude to each station. When the fireball altitude was improved in the next iterative step, the average sound speed was also recomputed. The real measured temperature profile (see next section) was used to compute sound speeds, and in these computations, the wind was ignored.

The azimuth and slope of the trajectory compare favorably to the values found from video reductions. The altitude, however, is closely related to the time (t_0) and both parameters could not be determined simultaneously with good precision. We, therefore, used the observed satellite time of the fireball (cf., Borovička et al. 2003a) 11:51:52.5 as t_0 . The other resulting parameters were as follows: 18.482° longitude, 31.7 km high, 172.0° azimuth of the ground path, 19.8° slope in the atmosphere (from horizontal), and 8.3 km/s velocity. The deceleration could not be reliably determined; the beginning point lies only 1.5 km west and 300 m below the video trajectory; the slope is within 1° of the video data, and the azimuth differs by 3.5° . The velocity differs significantly from the video value of 18 km/s at 32 km altitude. Except for the velocity, we obtained reasonable results, even ignoring wind corrections. We also ignored the fact that the fireball consisted of a number of laterally separated fragments. Our good agreement with the video-determined trajectory demonstrates that the cylindrical blast wave was clearly present, while the recording of numerous sub-maxima in the seismic amplitude (cf., Borovička and Kalenda [2003] for details) establishes the presence of acoustic energy from several fragmentation events producing quasi-spherical shocks.

THE INFRASONIC DATA

The detection of infrasonic waves from fireballs has been reported extensively in the past (e.g., ReVelle 1976, 1997; Evers and Haak 2001; Brown et al. 2002a). However, in very few cases have details of the trajectory, velocity, and fragmentation behavior of the associated fireball been

Table 2. Seismic waves first arrival times at different stations.^a

	CSM	RAJ	LUT	PRS	BMZ	HAV	CHO	MAJ	CSA	KVE
P term	ND	ND	ND	ND	ND	ND	ND	ND	ND	ND
Rayleigh (R → P)	ND	93.6	96.2	98.1	124	ND	ND	90	ND	ND
Direct-air (DA → P)	90.1	96.4	100.9	102.8	129.1	ND	ND	92.95	95.26	90.4
	RAC	OJC	MORC	VRAC	KRUC	JAVC				
P term	56.4 ^b	NS	75.3	81.5 ^c	NS	NS				
Rayleigh	128.4	NS	245	182 ^c	NS	248				
Direct-air	137.7	338.9	245.5	NA	NA	NA				
Direct-air term	NA	NA	NA	NS	503*	307.9				

^aThe time is given in seconds after 11:51:50 UT. ND = no data at the time of expected first arrival; NS = wave not seen in the data; NA = not applicable. For the underground stations (MAJ, CSA, KVE), the first arrival of Rayleigh and direct-air waves transformed to P-waves is given. The waves designated as “term” originate in the terminal point of the trajectory.

^bUncertain identification.

^cWeak signal near to the noise level.

available comparable to the Morávka fall. All these details offer potential insight into the source generation mechanism of the infrasound and permit us to estimate the source energy of the fireball from infrasonic records for comparison with other techniques.

Infrasonic signals associated with the Morávka event were recorded in Freyung, Germany by station FREYUNG (13.7131° E, 48.8516° N, $h = 1111$ m), which is part of the International Monitoring System (IMS) of the Comprehensive Test Ban Treaty (CTBT), at a distance of 360 km from the fireball endpoint (see Borovička et al. 2003a). The signals are shown in Fig. 4. The station recorded the airwave arrival from the fireball beginning 1182 sec after the fireball (12:11:32 UT) and ceasing approximately 308 sec later at 12:16:38 UT. To define the signal characteristics we examine the frequency spectrum of the original signal. This spectrogram is shown in Fig. 5. Here, we see that the signal is visible between 0.3 and 3 Hz; below 0.3 Hz, interference from microbaroms overwhelms the bolide signal (cf., Evers and Haak [2001] for a description of microbaroms). Some signal energy in the most energetic portions of the wave train extends up to the Nyquist cutoff for the sensors near 9 Hz. To

define the portion of the record having clear signal energy from the event, we band pass the signals over the frequency range of 0.3–9 Hz and then perform a cross-correlation between the 4 microphones over 30 sec windows to define the direction (azimuth) to the signal maximum cross-correlation within each window bin. The cross-correlation result is shown in Fig. 6 together with the associated directions in Fig. 7. This beam-forming technique is described in detail in Evers and Haak (2001).

Phenomenologically, the signal consists of 3 major portions. The most obvious are the 2 signal wave trains, which are clearly visible in the filtered amplitudes (Fig. 4). The first of these major wave trains (train 1) coincides with the onset of the signal at 12:11:32 UT (1182 sec) and continues for approximately 43 sec ending near 12:12:15 UT (1225 sec) when the amplitude decreases almost to the ambient noise levels. We note, however, that the signal cross-correlation remains well above background levels during this amplitude minimum (Fig. 6), indicating the presence of continuing coherent acoustic energy from the fireball. This ongoing signal is also noticeable in the frequency spectra.

The main body of the signal begins near 12:12:37 UT (1247 sec) (train #2). Here, the peak amplitude of the entire signal occurs near 12:12:57 UT (1267 sec). The amplitude of train 2 returns to near noise levels beginning at 12:13:30 UT (1300 sec). However, the cross correlation remains at least one standard deviation above background for almost another 3 minutes after this time period, as can be seen in Fig. 6. Indeed, the azimuth directions to maximum cross-correlation shown in Fig. 7 indicate continued arrivals as seen at Freyung from 65–67° azimuth (azimuth is counted from north) during this interval beginning near 12:14:00 UT (1330 sec), which we designate as train #3. This arrival is visible almost exclusively in cross-correlation and in the azimuth records; little or no amplitude fluctuations above background are in evidence.

In addition to these data, Fig. 8 shows the trace velocity of the signal at maximum cross-correlation in each of the

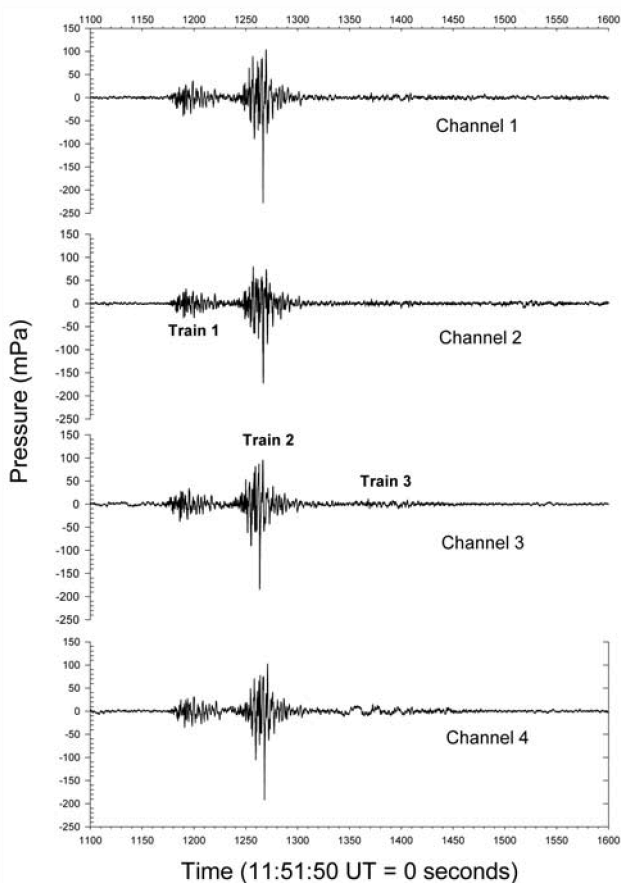


Fig. 4. The recorded infrasound signal on all 4 channels at Freyung for the Morávka fireball. Note that these waveforms have been band passed from 0.3–9 Hz to most clearly define the fireball signal.

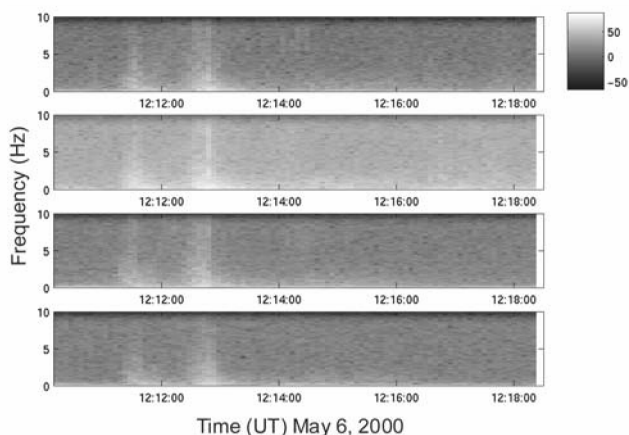


Fig. 5. Frequency spectrogram of all 4 channels (channel one at top, channel four at the bottom) of the infrasound array. The spectrogram grey-scale shows gradations in dB.

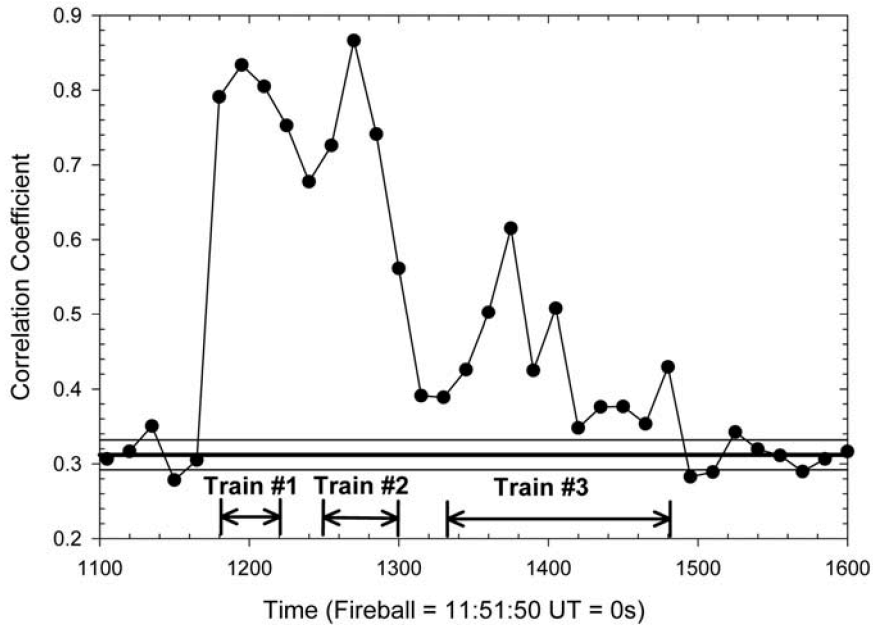


Fig. 6. The maximum correlation coefficient during the time centered around the Morávka fireball signal at Freyung. Windows of 30 sec (with 50% overlap per window) are used to define individual measurements of cross-correlation. The background cross-correlation in this frequency bandpass (0.3–9 Hz), calculated for the interval 3 minutes before the onset of the signal, is 0.31 ± 0.02 and is shown by a thick solid horizontal line (mean) and thin lines representing the range of the standard deviation.

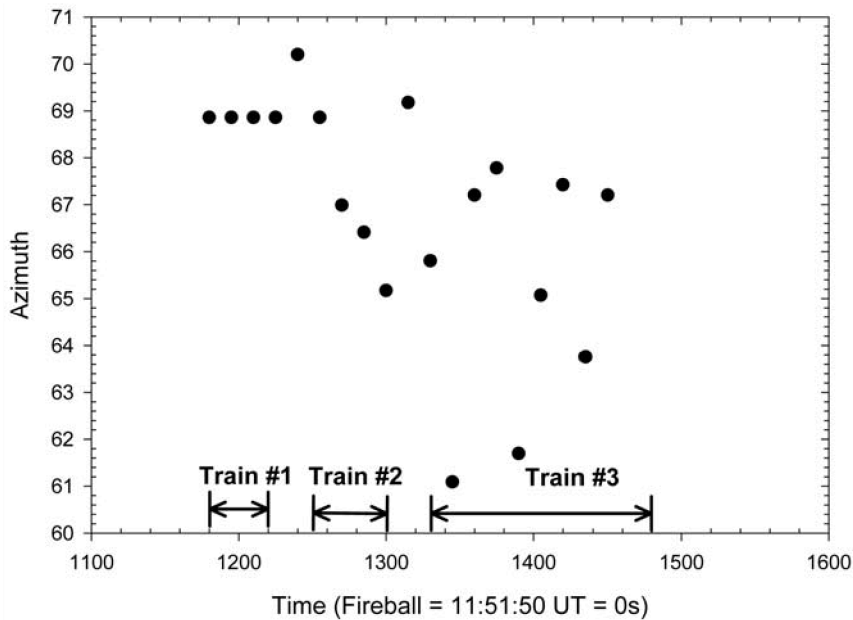


Fig. 7. Observed azimuths of infrasound arrival (north = 0) for each maximum in cross-correlation per bin.

30 sec window bins over the course of the entire fireball airwave. The trace velocity is a measure of the apparent velocity of travel of the signal from one microphone to the next; the steeper the arrivals, the higher the trace velocities. Here, we see that very little variation occurs in the trace velocities over trains #1 and #2, with a slight possible increase apparent over the duration of train #3. These wave train

signals are summarized in Table 3 along with times of maximum, peak amplitudes, and corresponding periods at maximum amplitude.

In the following sections, we will use 2 approaches to study the propagation of acoustic waves from the fireball trajectory to the station at Freyung to interpret these signals. First, we employ a purely analytical method for a line source

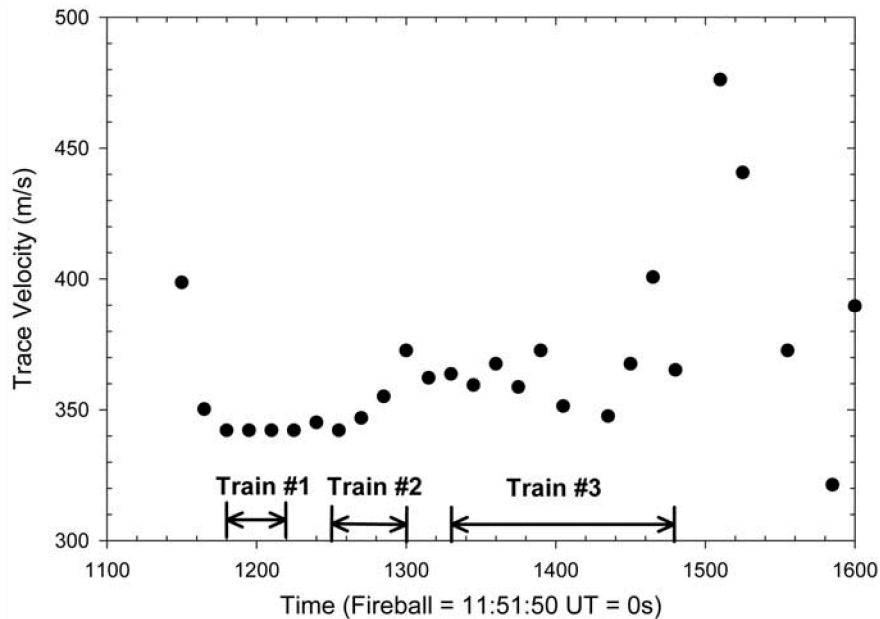


Fig. 8. Observed trace velocities of the infrasound for each maximum in cross-correlation per bin.

Table 3. Observed signal characteristics of the Morávka fireball as seen from Freyung, Germany on 6 May, 2000. The start and end times are referenced to 11:51:50 UT.

Wave-train	Start (sec)	End (sec)	Duration (sec)	Time of max (UT)	Azimuth	Peak amplitude (mPa)	Trace velocity (km/s)	Period (s)	Mean signal speed (km/s)
1	1180	1226	43	12:11:42	68.5 ± 0.7	63.8 ± 7.2	0.344 ± 0.003	3.2 ± 0.3	0.302–0.312
2	1247	1300	53	12:12:57	66.7 ± 2.8	233.3 ± 32.8	0.355 ± 0.013	4.1 ± 0.8	0.285–0.297
3	1325	1490	165	–	–	6 ± 3	0.353 ± 0.026	–	0.248–0.279

producing a cylindrical blast wave in a range-independent atmosphere. Next, a detailed numerical ray tracing approach is examined using moving point sources along the trajectory in a range-dependent model atmosphere.

INFRASONIC ANALYSIS FOR A CYLINDRICAL LINE SOURCE IN A RANGE-INDEPENDENT ATMOSPHERE

As a means of examining the infrasound propagation in a range-independent atmosphere, we can make use of the geometrical acoustics approximation (wavelengths that are small compared to the pressure scale height, the vertical scale over which significant atmospheric pressure gradients can occur) for which there are 2 constants of the motion in a horizontally stratified steady state atmosphere; that is, an atmosphere with perfect stratification. These constants are the heading of the wave normal (not the acoustic ray) from the source and the characteristic velocity (V_k) generated at the source. In this approximation, the arriving trace velocities at the array are the same as the V_k values at the initial source

heights at which they were generated. The characteristic velocity can be thought of as the horizontal propagation velocity modified for the effects of horizontal wind and entry geometry (see ReVelle [1976] for a complete discussion).

Here we have reproduced the cylindrical line source blast wave approach developed by ReVelle (1976). In this method, the characteristic velocity of the acoustic signal from the line source is calculated as a function of altitude throughout the known trajectory. Due to non-steady effects or imperfect stratification (range dependent atmosphere effects, etc.), the value of the characteristic velocity is expected to be modified during propagation. In Figs. 9 and 10, we have indicated the atmospheric structure parameters, the so-called effective acoustic velocity (the signal propagation velocity including winds), and the calculated characteristic velocity (V_k) for the range of observed back azimuths from the infrasonic detection at Freyung. These parameters are all discussed further by Cepelchka et al. (1998, p. 380).

To model these acoustic arrivals, we made use of the radiosonde data from Poprad, Slovakia (~150 km ESE from the fireball) at 12 UT on May 6, 2000 to define the

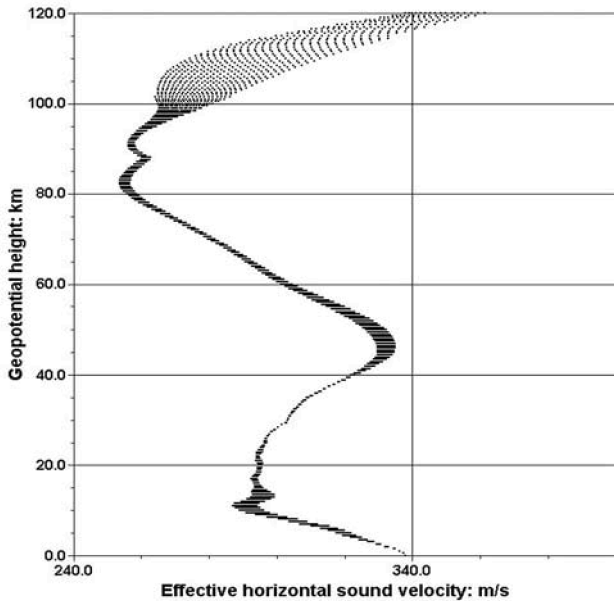


Fig. 9. Characteristic velocity as a function of height for the Morávka bolide modeled as a line source explosion along with the effective horizontal sound speed as a function of height (far left hand curve as indicated).

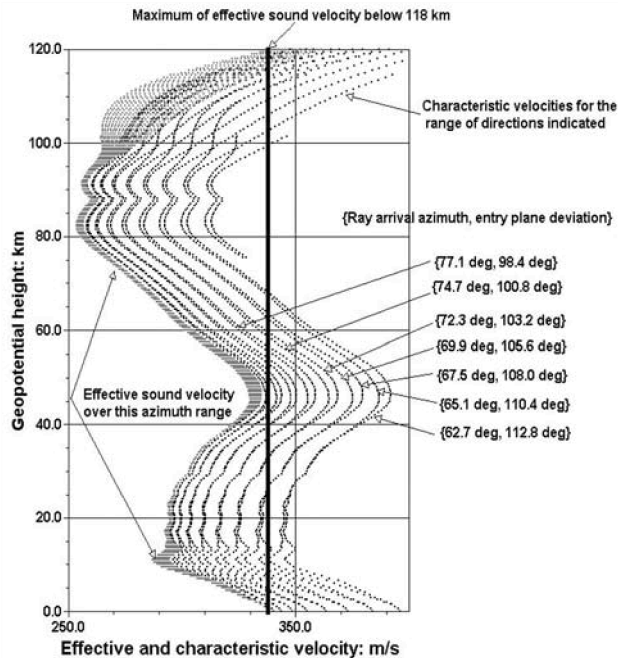


Fig. 10. Effective horizontal sound velocity versus height for “ray” paths from the Morávka trajectory over a range of azimuths (62.7° to 77.1°) towards Freyung.

temperature and wind field up to 30 km in altitude. Above 30 km, we merged these radiosonde data with the MSIS-E (Mass Spectrometer and Incoherent Scatter model) to produce the temperature profile (cf., Picone et al. 1997) to a height of 140 km, inputting the appropriate geomagnetic indices for

May 6, 2000. These indices significantly affect the atmospheric temperature and, thus, sound speed at heights above ~100 km. The wind field above 30 km uses the HWM (Horizontal Wind Model) (Hedin et al. 1996).

The propagation criterion within the geometrical acoustics approximation can be stated simply. Whenever the characteristic velocity at the source exceeds the maximum effective horizontal sound velocity over a given height interval, “rays” will refract in such a way that they will reach the ground (with sound waves bending away from regions of increasing temperature/increasing sound speed gradients).

As indicated in Fig. 10, for the altitude region from the ground to ~118 km, the maximum effective horizontal sound speed is equal to 347 m/s for our atmospheric conditions. For those “rays” that have a V_k value greater than this value, “ray” paths exist between the line source sound generation altitudes and points on the ground, though in general, only a small subset will reach any given location (i.e., Freyung in our case).

Since the line source is a complicated acoustic ray generation source, we will first describe briefly the acoustic radiation pattern. In all cases where the velocity of the meteoroid is much higher than the local sound speed, the radiation is perpendicular to the trajectory. The only region where this is not quite correct is near the bolide end height where the Mach cone opens up substantially as the meteoroid is heavily decelerated shortly before the onset of dark flight and the fall of meteorites toward Earth. Within the entry plane, the vertical plane containing the trajectory that has a normal that is tangent to the earth’s surface immediately below the mid-point of the fireball path, the rays travel in exactly opposite azimuth to the heading of the bolide, i.e., toward 355.5° (from the north) and have a downward component. At the same time, rays exist at all heights with an upward motion the heading of which is the same as the bolide, i.e., 175.5°, but these do not generally reach the ground near the region of the fall ellipse and have not been examined here. As the downward rays outside of the entry plane are examined and we consider additional propagation directions, we find that the ray headings turn progressively toward less northerly directions as the ray launch angle becomes less steep. Eventually, as seen in Fig. 11, the ray launch angle goes to zero (horizontally launched rays) at right angles to the trajectory.

Beyond this angle, the rays have no initial downward component. As further angular deviations from the entry plane are considered, rays are launched at progressively larger horizontal launch angles with an initial upward component to their motion. At horizontal launch angles of ~15–30° and angular deviations from the entry plane of 110–115°, i.e., 20–25° degrees above the horizontal, the proper initial launch directions are reached to enable rays to propagate to Freyung (arrival azimuths to Freyung of ~75–60° where the arrival azimuth is equal to the bolide heading (175.5°) minus the angular entry plane deviation). Note that these rays travel

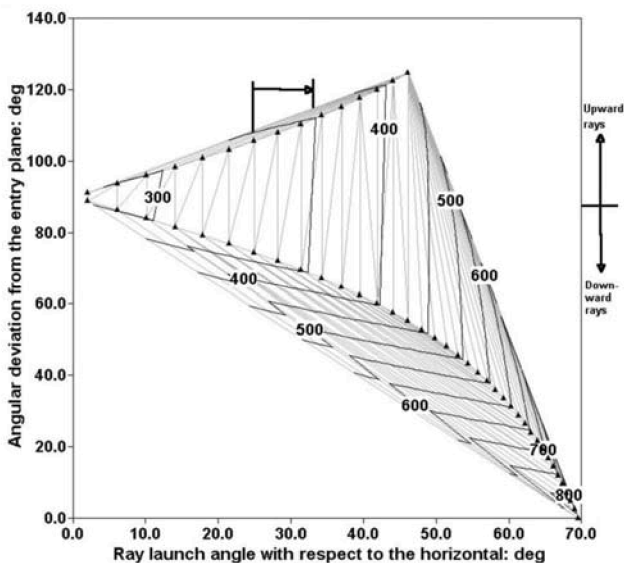


Fig. 11. Contoured line source characteristic velocities (V_k) (m/s) for a source height of 35 km for Morávka as a function of the horizontal “ray” launch angle and the angular deviation from the entry plane. A deviation of 90° is the dividing line between possible initial “ray” launch angles with upward (downward) paths for deviations $>90^\circ$ ($<90^\circ$). Possible “ray” paths to Freyung are indicated by the arrow for angular deviations from ~ 110 – 115° and corresponding upward “ray” launch angles ~ 25 – 32° . The triangles represent computed V_k values and the labeled (connected) lines are the resulting contour values for V_k . The horizontal arrow shows the range of launch deviations and angular deviations for arrivals that could be observed at Freyung.

upward first and are refracted downward by the zone of very large sound speed in the lower thermosphere. These are the only rays predicted to arrive at Freyung by the cylindrical line source model.

We summarize the predicted cylindrical line source behavior by taking the vertical line from the ground effective sound speed value until it crosses each of the respective V_k contour lines for each direction with the minimum V_k value equal to ~ 347 m/s in Table 4.

Having established that the only possible returns from a line source for Morávka are rays launched upward initially and subsequently arriving after refraction from the lower thermosphere below ~ 118 km (see also Fig. 14, path 4), we may estimate the region along the fireball trajectory from which rays might be generated. Our predicted lowest source heights for signal azimuths from 63 – 70° for Morávka, as seen at Freyung, are largely ~ 28 km in reasonable agreement with the moving point source (see next section) and seismic results. We emphasize that the cylindrical line source model does not show any downward stratospheric-type returns, even though that such rays are observed in the infrasound seems indisputable (see below).

Based on these calculations, we plot the V_k value as a function of the horizontal launch direction and of the entry plane deviations as shown in Fig. 11. The computed line

Table 4. Possible infrasonic arrivals to Freyung from analytical solutions in the line source geometry and range-independent atmosphere.

Azimuth arrival angle at Freyung (deg)	Angular, entry plane deviation (deg)	Possible source altitudes (km)
62.7	112.8	10.0 ^a –69.5
65.1	110.4	0.0 ^a –69.0
67.5	108.0	28.0–65.0
69.9	105.6	28.0–64.0
72.3	103.2	34.5–59.5
74.7	100.8	34.5–59.0
77.1	98.4	37.5–56.0

^aThe Morávka bolide did not maintain the necessary characteristics to be a line source explosion at such low heights.

source V_k values in Figs. 10 and 11 vary from ~ 350 – 366 m/s for source heights from ~ 28 – 36 km or 347 – 420 m/s over azimuths at Freyung from ~ 63 – 77° for all allowed source heights given in Table 4. The measured infrasonic trace speeds ($=V_k$ in a steady state, horizontally stratified atmosphere, assuming perfect stratification) are ~ 347 – 372 m/s for azimuths at Freyung from ~ 62 – 70.2° (see Figs. 7 and 8). These calculations indicate the possible degree of error inherent in infrasonic trace speeds at certain times, effects due to atmospheric range dependence, non-steady effects, local planetary boundary influences, or all of the above.

INFRASONIC ANALYSIS OF A MOVING POINT SOURCE IN A RANGE-DEPENDENT ATMOSPHERE

If a significant fragmentation along the fireball trajectory exists, we expect that some rays will be launched at angles other than purely normal to the trajectory. To investigate this scenario, we shot rays from each point along the trajectory below 40 km in the direction of Freyung but with a wide range of elevation angles. The rays were allowed to propagate through a steady state, model atmosphere that allows for range-dependence of atmospheric properties, i.e., imperfect stratification effects, including refraction in both the horizontal and vertical planes. The range dependence is present as a small change in the temperature (and thus, the sound speed) at each height within the MSIS model. Over the relatively short distance between the fireball and Freyung, however, this temperature change is on the order of 1° or less at most heights. Clearly, most of the differences between the results from this model and from the cylindrical line source model arise primarily from differing initial launch geometries for the rays involved.

We followed the complete acoustic path for each ray to determine the delay time and arrival direction at the receiver of those rays passing within 10 km horizontally or vertically and of the receiver array. The wind field and temperature profiles used are shown in Fig. 12, and the same atmospheric profiles were used as in the range-independent analysis earlier.

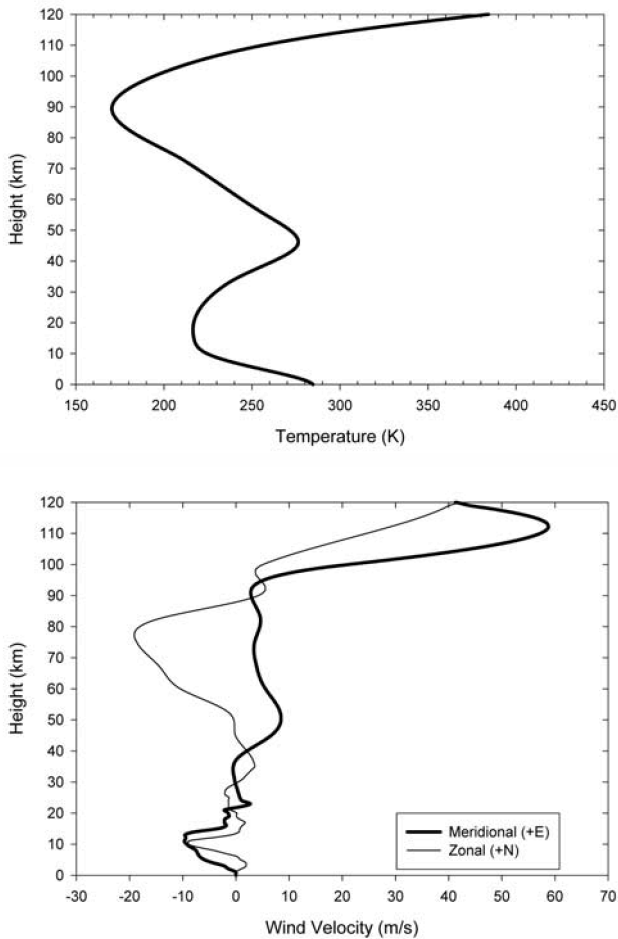


Fig. 12. Model atmospheric temperature profile (top) and wind field (bottom) used for numerical ray tracing and line source modelling.

In this numerical model, for a given elevation angle for each launched ray, the algorithm searches for ray paths beginning near the nominal great-circle azimuth between the point source along the fireball path and Freyung. At each iteration, the closest approach distance between a test ray at some launch azimuth and the receiver (Freyung) is determined and another ray at a slightly different azimuth is chosen in an attempt to decrease this distance and so forth. This iterative process continues until a ray launch azimuth is found that meets the arrival criteria at Freyung or some specified number of iterations made without success (typically on the order of several hundred at each launch elevation). This technique is used to find the full range of possible acoustic paths between each point along the fireball trajectory and Freyung without any predetermination of the source characteristics.

The results of these acoustic runs are shown in Fig. 13. From the figure, the modeled delay times clearly produce several sets of distinct arrivals at Freyung. First, an early set of model arrivals near 1180 sec corresponds well to the first observed maxima (train #1) in the amplitude record. Second,

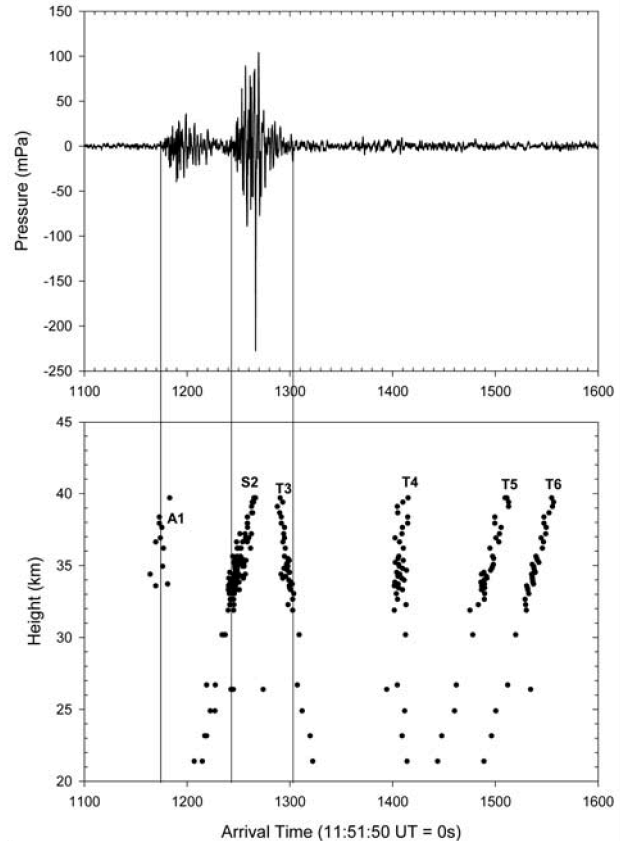


Fig. 13. Modeled arrival times as a function of source height along the fireball trajectory (lower plot) compared to the observed signal amplitude at Freyung (top). The acoustic branch identifications given in the lower plot follow the convention used in Figs. 14 and 16 with (A) representing the anomalous “leaky-duct” path, (S) stratospheric paths, and (T) thermospheric returns.

2 major sets of acoustic arrivals starting at 1200 sec and 1330 sec at low heights along the fireball trajectory and crossing near 1280 sec at a source altitude of 42 km represent the second and largest maxima, train #2. Finally, 3 distinct sets of arrival pathways beginning just before 1400 sec and continuing until 1550 sec correspond to the weaker train #3. We will examine each of these arrival paths and label them chronologically from 1–6.

The first of these paths (path 1) arrives with mean signal speeds near 0.31 km/s, intermediate between the speeds expected of tropospheric and stratospheric returns (cf., Cepelcha et al. 1998, p. 384). From Fig. 13, these modeled arrivals are perhaps 10–20 sec earlier than the main signal for train #1, though they correspond with the beginning of the signal at Freyung. For the given travel times of ~1200 sec, these errors amount to 1–2%, which is a remarkable agreement given our approximations in the modeled atmosphere. Figure 14 shows a typical arrival ray for this acoustic path.

Clearly, this is an unusual ray path that resembles rays that “leak” from the stratospheric waveguide and, in so doing,

have shorter paths and, thus, higher average signal velocities than normal stratospheric returns (cf., Arase [1959] for an example of this effect in the ocean). These waves propagate parallel to the Earth's surface at the top of the stratospheric duct and "leak" back to the surface. In previous work, the inclusion of explicit range dependence of temperature typically results in these types of acoustic arrivals. From our simulation results, the source heights responsible for this infrasound return are restricted to the interval from 34–40 km altitude along the fireball trajectory.

We have found that removing the range dependence of the atmosphere does not remove this acoustic path. Instead, we were able to find this arrival only by searching with very fine steps (0.1°) in our numerical ray launch elevations modeled within the framework of a moving point source. For a given height, only a very small range of launch angles produces this anomalous arrival path between the fireball and Freyung, as shown in Fig. 15. We find that for precisely the proper launch angle, the ray paths appear to travel along the top interface of the stratospheric duct where the turning point at the local maximum in sound velocity is reached near 45 km altitude. We also observe that generation of acoustic energy over this height interval is independently confirmed by the measured arrival azimuth of 68.5° , which compares very favorably with our modeled range of ray arrival azimuths at Freyung for train #1 (67° – 69°).

For train #2, the mean signal speed near 0.29 km/s is

characteristic of stratospheric returns. Typical rays associated with these acoustic paths are shown in Fig. 14 as a group of paths labeled 2. Clearly, these paths are stratospheric arrivals corresponding to rays launched at slightly different downward angles along the flight trajectory. The timing of the arrivals relative to the source heights suggests sound generation primarily in the interval above 30 km. The time of maximum for train #2 suggests a possible maximum in sound production near ~ 38 km, though differences between the true atmosphere and our model atmosphere make this number uncertain by at least several km. The thermospheric path 3 also has an arrival time consistent with contribution to train #2, but this return is likely very weak (see below).

The final signal train (#3) has a mean signal velocity near 0.25 km/s, which is representative of thermospheric returns. Figure 14 shows the thermospheric ray arrivals typical of paths 4–6. Clearly, all these paths represent thermospheric returns. For thermospheric returns to be the weakest of all infrasonic signals is not uncommon due to the high signal absorption at the top of the thermospheric waveguide (cf., Beer [1974] for a detailed discussion). One of these arrivals (path 5) is an extremely high thermospheric arrival with concomitantly high attenuation. Thus, path 5 probably contributes little or not at all to the thermospheric signals. For the same reason, path 3 probably does not contribute significantly to train #2.

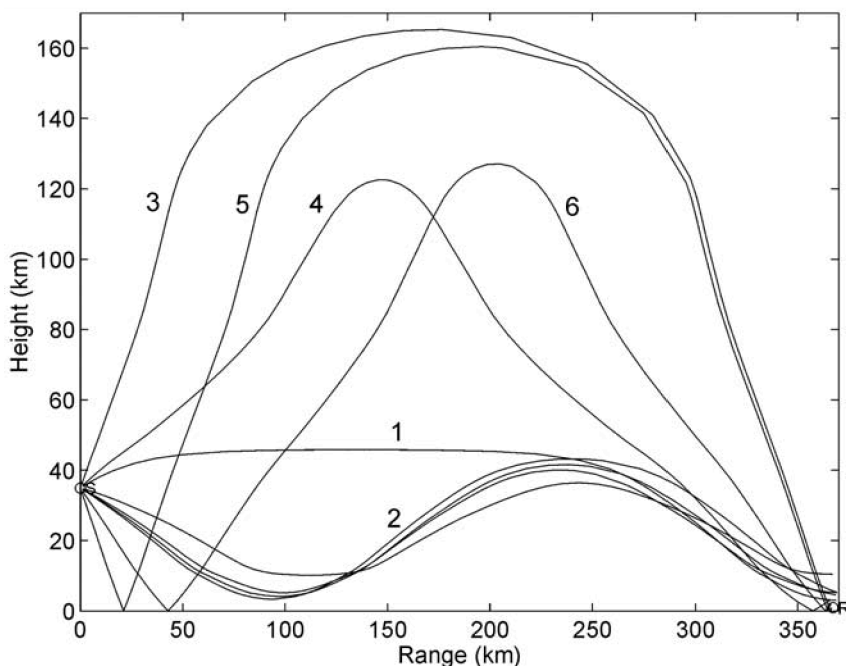


Fig. 14. Examples of acoustic ray propagation from the fireball trajectory (here a point at 35 km altitude) to the station Freyung. Path 1 is confined to the top of the stratospheric channel (near 45 km altitude) and then leaks to the receiver. This is the mode of propagation for the signals associated with the observed train #1. The paths labeled 2 are confined to the stratospheric channel (between 5 km and 45 km) and form the train #2. Paths 3–6 are confined to the thermospheric channel (between ground level and 120–160 km). Path 3 may contribute to train #2, while paths 4–6 form train #3.

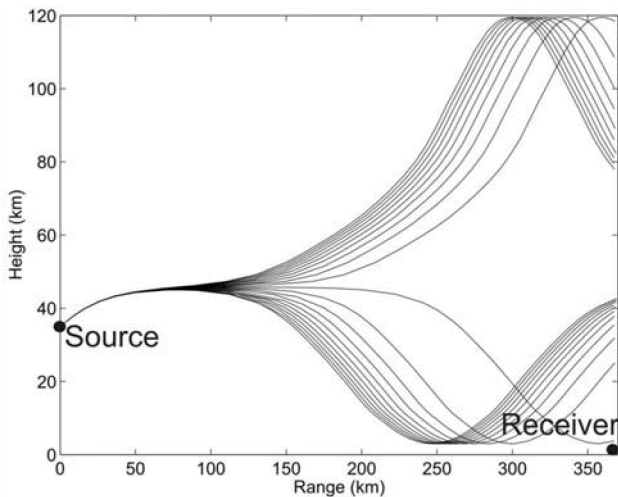


Fig. 15. Ray paths from point source at 35 km near elevation launch angle needed to form leaky duct solutions. Here each ray is launched and incremented 0.1° in elevation relative to its neighbor. The change between stratospheric, leaky duct and thermospheric arrivals occurs over less than 0.3° difference in launch elevation at the interface. This demonstrates the sensitive dependence of this solution on precisely the right launch angle for this particular height and our adopted atmospheric parameters.

One puzzling aspect of the signal of train #3 is its low trace velocity (see Table 3). In general, we expect thermospheric returns to be steeper than stratospheric returns with higher trace velocities. This points to the fact noted in McIntosh and ReVelle (1984) that the elevation arrival angle, measured by the horizontal trace velocity, is inherently less reliable as a parameter than is the plane wave back azimuth. This is due, in part, to local meteorological effects, which, at times, can change the elevation arrival angle considerably. Similar trace velocities are also found for other Morávka arrivals that have been ducted between the ground and the upper stratosphere and between the ground and the lower thermosphere, so we are very confident that the measurements are correct. The inherent error in these trace velocity values is certainly larger than that inferred by the measured standard error (see McIntosh and ReVelle [1984] for a more complete discussion of this effect).

We also caution that the individual ray arrival times computed here are, in reality, the center of a wave train emitted by each moving point source along the trajectory, in the context of our modeling. This wave train experiences dispersion along the propagation route (not taken into account in our geometric ray approximation), which acts to smear out the overall signal, yielding the longer wave trains actually observed.

Figure 16 shows the deviations of individual rays from the direction perpendicular to the fireball trajectory. Only the rays corresponding to path 4 and launched at heights of $\sim 25\text{--}35$ km are sufficiently close to the perpendicular direction to be considered part of the cylindrical blast wave. This confirms the finding of the previous section that only

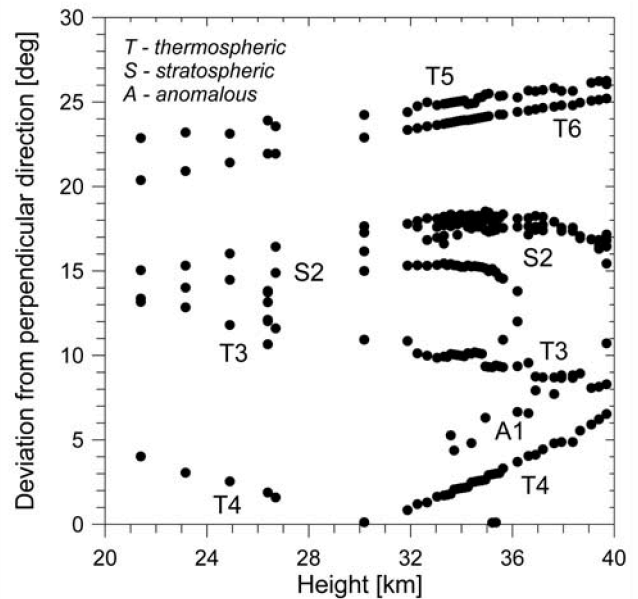


Fig. 16. The deviations of the individual ray launch directions from the direction perpendicular to the fireball trajectory plotted as a function of source height along the fireball trajectory. The rays are marked by signal types (thermospheric, stratospheric, anomalous) and path numbers (see Figs. 13 and 14).

thermospheric returns are possible at Freyung from a cylindrical line source. As outlined in this section, however, the strongest infrasonic signal at Freyung (train #2) was produced by stratospheric returns from a moving point source, which we interpret to be, most likely, individual fragmentation events.

The analysis of the video and seismic data for Morávka, presented in Borovička and Kalenda (2003), shows that a large number of fragmentation events clearly occurred between 29–37 km, lending further support to this interpretation. We note that train #1 also was produced by a moving point source as the deviation from the perpendicular direction was larger than ~ 5 degrees. The fact that much of the signal detected at Freyung was caused by fragmentation events is not sufficient to conclude that, in overall terms, fragmentation was the main source of sounds associated with the fireball. In fact, the geometric configuration and actual atmospheric conditions may have led to preferential detection of acoustic energy produced from point sources at the particular location of Freyung. The propagation of cylindrical line source energy to Freyung would be greatly attenuated due to the thermospheric nature of any such signals.

In summary, we find that at least 3 distinct sound “channels” provided signals at Freyung. The 2 stratospheric channels dominate the signal energy, but noticeable energy from thermospheric returns is also recorded late in the record. The earliest arrival is notable as being due to leaky-duct-type propagation, not normally recorded for atmospheric explosions.

CONCLUSIONS

Acoustic energy from the Morávka fireball was generated at the source as both a cylindrical line source blast wave and from fragmentation events (which we term an extended line source) in the height interval of ~30–40 km, with a probable maximum for the fragmentation-produced sound near 38 km, as measured at the location of Freyung. These conclusions are consistent with the results of Borovička and Kalenda (2003), who measured directly the fragmentation as occurring primarily between 29–37 km altitudes.

The direct arrival of the cylindrical line source blast wave produced the strongest signal on seismic stations located on both sides of the fireball trajectory. Stations located up range of the fireball terminal point registered the arrival of a nearly spherical blast wave propagating from the terminal point. However, the first, though weaker, waves arriving at all stations were air-coupled P-waves. These are sonic waves transformed to the ground P-waves and propagating quickly near the surface of the Earth, as described in Brown et al. (2002b). The first waves originated at the fireball terminal point, i.e., the lowest point of the trajectory, and the P-waves were followed by directly-coupled airwaves and larger amplitude Rayleigh waves.

The seismic record also contains signatures of individual fragmentation events. The fragmentations mimicked small explosions and formed quasi-spherical shock waves. Deep underground stations also detected the seismic signature of the fireball. Reconstruction of the trajectory of the fireball was possible, based on seismic data alone, to accuracies of 1° in elevation of the fireball radiant and 3.5° in the azimuth of the radiant as compared to the video-determined trajectory (Borovička et al. 2003a). This demonstrates the expected accuracy in seismic-only trajectory solutions. Somewhat better precision might be obtained by including winds in the solutions to modify the effective sound velocity.

The propagation of sound to larger distances was governed mostly by the geometry of the trajectory combined with the actual atmospheric conditions. At Freyung, an infrasonic station located 360 km from the fireball, 3 distinct signal trains were measured. The cylindrical blast wave may have contributed only the weakest signal by a refraction of sound in the thermosphere at the height of ~120 km. The strongest signal must have been produced by moving point sources along the trajectory, i.e., by the individual fragmentation events, and recorded at the receiver by double refraction at the heights of 5 and 45 km. The deviations of the acoustic ray launch angles from the perpendicular in these fragmentation events was found to be between 5°–30° as seen from Freyung, substantially larger than the few degrees of deviation expected from a purely cylindrical line source model. The first signal arrival was propagating through the stratosphere horizontally and then leaked to the receiver. This is the first time, to our knowledge, that such an anomalous

hybrid horizontal-stratospheric mode of acoustic propagation has actually been observed for an atmospheric source.

Acknowledgments—Seismic data were provided by J. Holecko (DPB Paskov), J. Pazdirkova (Masaryk University Brno), P. Wiejacz (Institute of Geophysics, Polish Academy of Sciences), and W. Wojtak (Silesian Geophysical Observatory, Raciborz); infrasonic data and calibration information were kindly sent by G. Hartman (German Federal Institute for Geosciences and Natural Resources, Hannover). Supporting meteorological data were obtained from J. Lukacko (Slovak Hydrometeorological Institute, Ganovce), P. Zarsky, and M. Setvak (Czech Hydrometeorological Institute, Praha). Infrasonic modeling of point sources was done using the Inframap utility developed by BBN technologies; a special thanks to D. Norris for providing support with this modeling. P. G. Brown acknowledges support in the form of a director-sponsored post-doctoral fellowship at Los Alamos National Laboratory. P. Jenniskens provided valuable comments on an earlier version of this manuscript.

Editorial Handling—Dr. Donald Brownlee

REFERENCES

- Anglin F. M. and Haddon R. A. W. 1987. Meteoroid sonic shock-wave-generated seismic signals observed at a seismic array. *Nature* 328:607–609.
- Arase T. 1959. Some characteristics of long-range explosive sound propagation. *Acoustical Society of America Journal* 31:588–595.
- Beer T. 1974. *Atmospheric waves*. New York: Halsted Press. p. 315.
- Borovička J., Spurný P., Kalenda P., and Tagliaferri E. 2003a. The Morávka meteorite fall. 1. Description of the events and determination of the fireball trajectory and orbit from video records. *Meteoritics & Planetary Science*. This issue.
- Borovička J., Weber H. W., Jopek T., Jakeš P., Randa Z., Brown P. G., ReVelle D. O., Kalenda P., Schultz L., Kucera J., Haloda J., Týcová P., Frýda J., and Brandstätter F. 2003b. The Morávka meteorite fall. 3. Meteoroid initial size, history, structure, and composition. *Meteoritics & Planetary Science*. This issue.
- Borovička J. and Kalenda P. 2003. The Morávka meteorite fall. 4. Meteoroid dynamics and fragmentation in the atmosphere. *Meteoritics & Planetary Science*. This issue.
- Brown P., Whitaker R. W., Rodney W., ReVelle D. O., and Tagliaferri E. 2002a. Multi-station infrasonic observations of two large bolides: Signal interpretation and implications for monitoring of atmospheric explosions. *Geophysical Research Letters* 29:14–14–4.
- Brown P., ReVelle D. O., Tagliaferri E., and Hildebrand A. R. 2002b. An entry model for the Tagish Lake fireball using seismic, satellite, and infrasonic records. *Meteoritics & Planetary Science* 37:661–676
- Cepelcha Z., Borovička J., Elford W. G., ReVelle D. O., Hawkes R. L., Porubčan V., and Šimek M. 1998. Meteor phenomena and bodies. *Space Science Reviews* 84:327–471.
- Cevolani G. 1994. The explosion of the bolide over Lugo di Romagna (Italy) on 19 January 1993. *Planetary and Space Science* 42:767–775.
- Cumming G. L. 1989. Alberta bolide of June 1, 1982: Interpretation

- of photographic and seismic records. *Canadian Journal of Earth Sciences* 26:1350–1355.
- Evers L. and Haak H. 2001. Sounds from a meteor and oceanic waves. *Geophysical Research Letters* 28:41–44.
- Folinsbee R. E., Bayrock L. A., Cumming G. L., and Smith D. G. W. 1969. Vilna Meteorite—Camera, visual, seismic, and analytic records. *Journal of the Royal Astronomical Society of Canada* 63: 61–86.
- Hedin A. E., Fleming E. L., Manson A. H., Schmidlin F. J., Avery S. K., Clark R. R., Franke S. J., Fraser G. J., Tsuda T., Vial F., and Vincent R. A. 1996. Empirical wind model for the upper, middle, and lower atmosphere. *Journal of Atmospheric and Terrestrial Physics* 58:1421–1447.
- Ishihara Y., Tsukada S., Sakai S., Hiramatsu Y., and Furumoto M. 2001. Determination of the fireball trajectory using dense seismic arrays. *Bulletin of the Earthquake Research Institute University of Tokyo* 76:87–92.
- McIntosh B. A. and ReVelle D. O. 1984. Traveling atmospheric pressure waves measured during a solar eclipse. *Journal of Geophysical Research* 89:4953–4962.
- Picone J. M., Hedin A. E., Coffey S. L., Lean J., Drob D. P., Neal H., Melendez-Alvira D. J., Meier R. R., and Mariska J. T. 1997. The Naval Research Laboratory Program on empirical models of the neutral upper atmosphere. In *Advances in the astronomical sciences*, edited by Hoots F. R., Kaufman B., Cefola P. J., and Spencer D. B. San Diego: American Astronomical Society. 2184 p.
- Qamar A. 1995. Space shuttle and meteoroid-tracking supersonic objects in the atmosphere with seismographs. *Seismological Research Letters* 66:6–12.
- ReVelle D. O. 1976. On meteor-generated infrasound. *Journal of Geophysical Research* 81:1217–1240.
- ReVelle D. O. 1997. Historical detection of atmospheric impacts of large super-bolides using acoustic-gravity waves. *Annals of the New York Academy of Sciences* 822:284–302.
-